Mon. Not. R. Astron. Soc. **000**, 000–000 (0000) Printed 16 April 2015 (MN LATEX style file v2.2)

New age-metallicity diagnostic diagram for the Washington photometric system

Andrés E. Piatti[1,2⋆], Gabriel I. Perren[2,3]
[1] *Observatorio Astronómico, Universidad Nacional de Córdoba, Laprida 854, 5000, Córdoba, Argentina*
[2] *Consejo Nacional de Investigaciones Científicas y Técnicas, Av. Rivadavia 1917, C1033AAJ, Buenos Aires, Argentina*
[3] *Facultad de Ciencias Astronómicas y Geofísicas, Universidad Nacional de La Plata, Paseo del Bosque s/n, 1900 La Plata, Argentina*

16 April 2015

ABSTRACT

The age calibration of the Washington δT_1 index is mainly used to estimate ages of star clusters older than 1 Gyr, no age-metallicity degeneracy effect is considered. We have profusely exploited synthetic T_1 versus $C - T_1$ colour magnitude diagrams aiming at exploring the intrinsic behaviour of the δT_1 index. The analysis shows that δT_1 varies with age and metal content as well. In general, the dependence on age weakens for ages greater than $\sim$ 6 Gyr, and results even less sensitive to age as the metallicity decreases. For ages younger than $\sim$ 5 Gyr δT_1 shows a strong correlation with both age and metallicity. The δC index -defined as δT_1 for the C passband- is also a combined measurement of age and metallicity. We introduce a new age-metallicity diagnostic diagram, δT_1 versus δC - δT_1, which has shown the ability of unambiguously providing age and metallicity estimates, simultaneously. The new procedure allows to derive ages from 1 up to 13 Gyr and metallicities [Fe/H] from -2.0 up to +0.5 dex, and is independent of the cluster reddening and distance modulus. It does solve the constraints found in the δT_1 index and surpasses the performance of the standard giant branch metallicity method. All these features make the diagnostic diagram a powerful tool for estimating accurate ages as well as metallicities.

Key words: techniques: photometric

1 INTRODUCTION

Geisler et al. (1997, hereafter G97) provided a calibration for the magnitude difference (δ) between the giant branch clump in intermediate-age star clusters (the horizontal branch in old clusters) and the main sequence turnoff as a function of the cluster age for the Washington photometric system. Particularly, they used the T_1 versus $C - T_1$ colour magnitude diagram (CMD) (effective wavelengths: $C \sim 3900$Å, $T_1 \sim 6300$Å; Canterna (1976)) of six known star clusters (ages $\gtrsim$ 1 Gyr) in order to measure δT_1 and fitted those values with the clusters' ages (see their Fig. 5 and eq. 4). δT_1 emulated the former δV index defined by Phelps, Janes & Montgomery (1994). By using such a calibration G97 firstly searched for old star clusters in the Large Magellanic Cloud; the 25 candidates analysed resulted to be of intermediate age (1-3 Gyr). Since then, the δT_1 index was employed successively to estimate the ages of star clusters in the Milky Way (e.g. Piatti, Clariá & Ahumada 2004), in both Magellanic Clouds (e.g. Bica et al. 1998; Piatti et al. 2001) and to derive ages for the so-called representative stellar population of galactic star fields (e.g. Piatti, Geisler & Mateluna 2012), among others.

The age calibration of the δT_1 index is based on CT_1 photometry of NGC 2213 and ESO 121-SC03 in the Large Magellanic Cloud and the Galactic open clusters NGC 1245, Tombaugh 2, M 67 and NGC 6791. At the very least the calibration needs revision, since updated ages and metallicities for the calibration clusters are available. For instance, Anthony-Twarog, Twarog & Mayer (2007) derived an age of (7.0 ± 1.0) Gyr for NGC 6791 ([Fe/H]=(+0.42±0.05) dex Heiter et al. 2014), whereas a value of 10 Gyr was used by G97. Except for ESO 121-SC03 ([Fe/H]=(-0.93±0.20) dex Olszewski et al. 1991), all of these calibration clusters are considerably more metal-rich than [Fe/H] $\sim$ -0.5 dex. In addition, the solar abundance cluster M 67 plays a pivotal role in the calibration as it is the only cluster in the 2-9 Gyr range. Secondly, thinking in the impact that the adopted cluster fundamental parameters can have on the former age calibration of the δT_1 index, it seems necessary to enlarge the cluster sample in order to support a robust relationship and to allow an analysis about the possible metallicity sensitivity

⋆ E-mail: andres@oac.uncor.edu

and the effect any such sensitivity might have on the derived ages. Nowadays, however, a representative sample of clusters with age and metallicity values distributed well along the known cluster age/metallicity regime and with Washington CT_1 photometry is not available. Given the usefulness that δT_1 has shown in the literature as a cluster age indicator, the above constraints seriously blur its full scope.

Fortunately, synthetic cluster CMDs are powerful tools to probe the genuine performance of δT_1 as an age indicator and to disentangle any metallicity dependence. This is because they can accurately reproduce CMDs of clusters of any age and metallicity, bearing in mind the fraction of binaries, the cluster initial mass function, the cluster mass, as well as photometric uncertainties and completeness effects, etc (Popescu, Hanson & Elmegreen 2012; Casagrande & VandenBerg 2014). In this sense, synthetic cluster CMDs have the advantage of representing those of calibration clusters with ages and metallicities derived on a homogeneous scale. Indeed, we have taken advantage of the recently developed Automated Stellar Cluster Analysis package (`ASteCA`[1] Perren, Vázquez & Piatti 2015), as we describe in Sect. 2 of this work, to profusely exploit a large number of synthetic cluster CMDs. From the outcomes of this comprehensive analysis, we present in Sect. 3 a new age-metallicity diagnostic diagram that involves δ values for the C and T_1 bandpasses. The proposed technique allows to estimate ages and metallicities for clusters older than 1 Gyr, independent of their reddening and distance moduli. Sect. 4 analyses the performance of the new procedure in the light of published accurate age and metallicity values as well as of different age and metallicity calibration for the Washington system. Finally, Sect. 5 summarises our main results.

2 SYNTHETIC COLOUR-MAGNITUDE DIAGRAMS

Synthetic stellar populations have usually been generated to study the astrophysical properties of different stellar populations through the comparison of their respective CMDs (e.g. Romeo et al. 1989; Hernandez, Valls-Gabaud & Gilmore 1999; Monteiro, Dias & Caetano 2010). The recovery of the star formation history of galaxies (Rubele et al. 2012), the study of the extended main sequence turnoff phenomenon in star clusters (Correnti et al. 2014), and the estimation of star cluster parameters (Donati et al. 2015) have been topics of astrophysical interest approached by synthetic CMD analyses. Likewise, synthetic CMDs offer the possibility to explore in detail the behaviour of different photometric indices in terms of astrophysical quantities (Catelan et al. 2014), to predict the range of distinct fundamental properties in star clusters (Popescu & Hanson 2014) as well as to assess in advance the performance of astronomical instruments (Kerber et al. 2009).

In order to revise the δT_1 age calibration and its possible dependence with the metal content, we have employed the `ASteCA` suit of functions to generate synthetic CMDs of star clusters covering ages from 1.0 up to 12.6 Gyr and metallicities in the range [Fe/H] = (-2.0 - +0.5) dex. `ASteCA` was designed as a new set of open source tools for an objective and automatic analysis of large cluster data sets. The code includes functions to perform cluster structure analysis, luminosity function curves, integrated colour estimates statistically cleaned from field star contamination, a Bayesian membership assignment algorithm, and a synthetic cluster-based best isochrone matching method to simultaneously estimate clusters' properties (age, metallicity, distance, reddening, mass and binarity). Perren, Vázquez & Piatti (2015) showed that it does not introduce any biases or new correlations between the various derived cluster parameter values.

The steps by which a synthetic cluster for a given set of age, [Fe/H], distance modulus $m - M$, and reddening $E(B - V)$ values is generated by `ASteCA` is as follows: i) a theoretical isochrone is picked up, densely interpolated to contain a thousand points throughout its entire length, including the most evolved stellar phases. ii) The isochrone is shifted in colour and magnitude according to the $E(B - V)$ and $m - M$ values to emulate the effects these extrinsic parameters have over the isochrone in the CMD. At this stage the synthetic cluster can be objectively identified as a unique point in the 4-dimensional space of parameters ($E(B - V)$, $m - M$, age and metallicity). iii) The isochrone is trimmed down to a certain faintest magnitude according to the limiting magnitude thought to be reached. iv) An initial mass function (IMF) is sampled in the mass range $[\sim 0.01-100]\, M_{\odot}$ up to a total mass value M_{total} provided via an input data file that ensures the evolved CMD regions result properly populated. Currently, `ASteCA` lets the user choose between three IMFs (Kroupa, Tout & Gilmore 1993; Chabrier 2001; Kroupa 2002) but there is no limit in the number of distinct IMFs that can be added. The distribution of masses is then used to obtain a properly populated synthetic cluster by keeping one star in the interpolated isochrone for each mass value in the distribution. v) A random fraction of stars are assumed to be binaries, which is set by default to 50% (von Hippel 2005), with secondary masses drawn from a uniform distribution between the mass of the primary star and a fraction of it given by a mass ratio parameter set to 0.7. Both quantities can be modified through the input data file. vi) An appropriate magnitude completeness and an exponential photometric error functions are finally applied to the synthetic cluster.

As for our purposes, we used the theoretical isochrones computed by Bressan et al. (2012) using extensive tabulations of bolometric corrections with uncertainties ~ 0.001 mag for the C and T_1 filters, the IMF of Chabrier (2001), and a cluster mass as a function of the cluster's age given by the expression $\log(M_{total}\ \mathrm{M}_{\odot}) = 1.8 \times \log(\mathrm{age\ yr}^{-1})$ - 12.8 (Baumgardt et al. 2013; de Grijs, Goodwin & Anders 2013; Piatti 2014) in order to keep not only the main sequence turnoff (MSTO) but also the red clump (RC) similarly populated as those of known low mass clusters. We considered no binarity effect, since it has been shown that binary stars can broaden the MSTO region (Li et al. 2012; Li, de Grijs & Deng 2013; Jiang, Han & Li 2014), in contrast with our aim of sizing up the sensitivity of the MSTO to age and metallicity. Fig. 1 shows some examples of the resulting synthetic CMDs. Note that the theoretical isochrones of Bressan et al. (2012) are in a very satisfactory agreement with another known set of isochrones for the Washington

[1] http://asteca.github.io/

system computed by Lejeune & Schaerer (2001) (e.g. Piatti et al. 2003, and references therein).

3 THE δT_1 INDEX

We measured the difference in magnitude between the MSTO and the RC in the generated synthetic CMDs following the precepts of Phelps, Janes & Montgomery (1994, see their Fig. 1), as G97 also applied in their definition of δT_1. The synthetic cluster CMDs allowed us to estimate the errors involved in measuring δT_1. We found that an uncertainty between 0.05-0.10 mag typically affects the measurements of δT_1, and can reach a few more hundredth of magnitude for some of the youngest clusters in our synthetic sample because of the shape of their MSTOs. Fig. 2 (upper left-hand panel) shows the resulting δT_1 values as a function of age for six different metallicity levels (coloured line scale). As can be seen, the relationship of δT_1 with age varies with the metal content as well. In general, the trend of δT_1 with the age weakens (it changes to a smaller slope) for ages larger than $\sim$ 6 Gyr, and results even less sensitive to age as the stellar population becomes more metal-poor ([Fe/H] $\lesssim$ -1.0 dex). This means that δT_1 does not result a good indicator of age independent of metallicity for old and metal-poor clusters. For ages younger than $\sim$ 5 Gyr δT_1 shows a strong correlation with both age and metallicity.

We included in Fig. 2 (upper left-hand panel) the relationship obtained by G97 represented by a solid black line. For ages younger than 3 Gyr they used three calibration clusters, two of them (NGC 2243, Tombaugh 2) have an average spectroscopic metallicity of [Fe/H] = (-0.4 $\pm$ 0.10) dex. Their δT_1 versus age relationship roughly matches the synthetic one for [Fe/H] = -0.5 dex. On the other hand, the older end of the G97's curve overlaps those of metal-poor clusters ([Fe/H] $\lesssim$ -1.5 dex). The upper right-hand panel of Fig. 2 illustrates clearer this metallicity dependence of δT_1 for twelve different age levels. Indeed, for δT_1 = 3.2 mag an age of 10.3 Gyr comes out from the G97's calibration as well as from synthetic CMDs with [Fe/H] $\lesssim$ -1.5 dex. However, an age $\sim$ 2.5 Gyr smaller results from the synthetic CMDs if a [Fe/H] $>$ -1.0 dex is adopted. Such a difference between mean age values results statistically significant even if we consider an uncertainty of 0.15 mag in the δT_1 values. Similarly, for δT_1 = 1.5 mag an age of 1.8 Gyr is derived from the G97's equation, or indistinctly from synthetic CMDs with [Fe/H] $\approx$ -0.6 dex. Once again, if [Fe/H] values of -0.1 dex and -1.1 dex were instead taken into account, the ages from synthetic CMDs would result 0.5 Gyr greater and 0.6 Gyr smaller than the G97's age, respectively; errors of 0.2 Gyr due to uncertainties in δT_1 were estimated.

The above examples not only illustrate that the δT_1 age index is sensitive to metallicity, but also that such a dependence is a complex function of both age and metallicity. Moreover, the age range for any particular δT_1 value obtained from the synthetic curves (see upper left-hand panel of Fig. 2) results many times larger than the age errors derived from eq. 4 of G97. Fig. 3 illustrates this trend for three different δT_1 error levels. This result points out to the need of a new calibration for the δT_1 age index which prevents us against any age/metallicity degeneracy.

We seek for any possible straightforward relationship between the δT_1 values derived from synthetic cluster CMDs, the age and the metallicity. Bearing in mind the kind of arithmetic expressions employed in previous δ age calibrations (Phelps, Janes & Montgomery 1994; Carraro & Chiosi 1994; Geisler et al. 1997; Salaris, Weiss & Percival 2004), we tried different possibilities which included linear, quadratic and terms of higher degree in any of the three quantities, mixed terms, logarithmic functions, etc. Note that we used a larger number of points than any previous δ age calibration, uniformly distributed throughout the whole age/metallicity range and without any constraint from non-homogeneity in the age/metallicity values. Unfortunately, we did not attain any satisfactory fit, which confirms the complex interdependence of the three parameters.

In order to complement this analysis and by taking advantage of the availability of magnitudes in the C passband (= T_1 + ($C - T_1$)), Fig. 2 (bottom panels) also depicts the relationship for δC - defined as δT_1 but for the C filter - with the age and the metallicity. In order to build that relationship, we first produced synthetic C versus $C - T_1$ CMDs for the same synthetic clusters used to construct the top panels of Fig. 2. Then, we measured the magnitudes at the MSTO and the RC and computed their difference (δC). The resulting curves show that δC expands over a dynamical range of $\sim$ 4 mag, similar to that of δT_1. However, although the overall appearance of δC and δT_1 curves look alike, the former show a less complex trend with age and metallicity. Particularly, they do not account for: i) the lack of metallicity sensitivity ([Fe/H] $>$ -1.0 dex) for stellar populations older than $\sim$ 5 Gyr and, ii) the slope change for clusters more metal-poor than [Fe/H] $\lesssim$ -1.0 dex. Nevertheless, Fig. 2 clearly suggests that δC is also a combined measurement of age and metallicity.

3.1 A new age-metallicity diagnostic diagram

At this point, we decided to introduce a new diagnostic diagram with the ability of unambiguously providing age and metallicity estimates within certain Washington CT_1 photometric error limits. We found that the plane δT_1 versus δC - δT_1 resulted to be the one which best distinguishes changes in age and metallicity throughout the whole two-dimensional space. In Fig. 4 we have traced iso-age lines and marked iso-abundance positions using colour-coded lines and filled circles, respectively. Errobars for typical uncertainties in δT_1 and δC - δT_1 are also indicated. Note that the iso-age lines and iso-metallicity positions rely on the theoretical isochrones used to build the synthetic CMDs, while the quoted errors refer to the uncertainty in measuring δC and δT_1 in observed cluster CMDs. In this sense, the capacity of resolving ages and metallicity varies with the position in that plane. Table 1 lists the age/metallicity errors associated to typical $\sigma(\delta T_1)$ and $\sigma(\delta C$ - $\delta T_1)$ uncertainties, derived by interpolation of Fig. 4. Particularly, we have highlighted with boldface characters those errors for (age, [Fe/H]) pairs that are within the ranges of the age-metallicity relationships (AMRs) of the Milky Way and of the Small/Large Magellanic Clouds (Beasley et al. 2004; Sabbi et al. 2009; Piatti & Geisler 2013). Since star clusters can have ages and metallicities directly linked to the chemical evolution history (AMR) of their host galaxies, the highlighted age/metallicity ranges in Table 1 result more usable from an astrophysical

point of view. We thickened the line sections in the δT_1 versus age diagram (see Fig. 5) corresponding to age/metallicity values with uncertainties in Table 1 in boldface. Thus, readers can consistently compare the G97 locus with the present theoretically-driven calibration according to known AMRs. Fig. 4 is aimed at entering with (δC-δT_1, δT_1) values and obtaining by interpolation age and metallicity estimates.

We used the new diagnostic diagram for clusters with high-quality CT_1 photometry, particularly with well-identified MSTOs and RCs, and with accurate ages and metallicities. We searched for metallicities obtained from high-dispersion spectroscopy, although in some cases we relaxed this requirement down to medium-dispersion spectroscopy or even to reliable photometric metal abundances. As for the cluster ages, we took advantages of those values derived from isochrones fitting to deep cluster CMDs. We excluded any previous age/metallicity estimates coming from Washington photometry.

From barely 340 clusters with published CT_1 data, we found nearly 150 with recognisable MSTOs and RCs. In general, the extracted cluster CMDs present signatures of contamination from the composite star field population along the line of sight. Such a field contamination does have a particular pattern given by the luminosity function, the colour distribution and the stellar density towards the cluster region. For these reasons, we first built CMDs representing the field along the line of sight towards the individual clusters, which we then used to clean the cluster CMDs with the aim of tracing fiducial cluster sequences as accurate as possible. We employed the cleaning procedure developed by Piatti & Bica (2012, see their Fig. 12). The method compares the extracted cluster CMD to four distinct CMDs composed of stars located reasonably far from the object, but not too far so as to risk losing the local field-star signature in terms of stellar density, luminosity function and/or colour distribution. Each field region covers an equal area as that of the cluster and the four field areas are placed to the north, east, south and west from the cluster.

The comparison of the cluster/field CMDs is performed using boxes of different sizes distributed in the same manner throughout both CMDs, thus leading to a more meaningful comparison of the numbers of stars in different CMD regions than using boxes fixed in size and position. The latter is not universally efficient, since some parts of the CMD are more densely populated than others. For instance, to deal with stochastic effects at relatively bright magnitudes (e.g., fluctuations in the numbers of bright stars), larger boxes are required, while populous CMD regions can be characterized using smaller boxes. Since the procedure is executed for each of the four field-CMD box samples, it assigns a membership probability (P) to each star in the cluster CMD. This is done by counting the number of times a star remained unsubtracted in the four cleaning runs and by subsequently dividing this number by four. For our purposes, we used stars that are predominantly found in the cleaned cluster CMDs ($P \geqslant 75\%$).

We used the cleaned cluster CMDs to measure C and T_1 magnitudes at the MSTO and RC, then computed δC and δT_1 and entered into the age-metallicity diagnostic diagram to estimate cluster ages and metallicities. The resulting values with their uncertainties for clusters that fulfilled the requirements mentioned above (e.g. available age/metallicity values from independent Washington techniques) are listed in the last columns of Table 2, in which we also included age/metallicity values adopted by thoroughly searching the literature for comparison purposes.

4 ANALYSIS

From the comparison between cluster ages taken from the literature and those estimated above (see Fig. 6) we obtained a mean age dispersion of $\Delta(\log(\text{age yr}^{-1}) = 0.07 \pm 0.02$ along the whole age range (1 - 13 Gyr). The resulting mean dispersion is slightly smaller than typical age errors ($\Delta(\log(\text{age yr}^{-1}) = 0.10$-$0.15$) derived from isochrone fitting to good-quality cluster CMDs, regarless of binarity, multiple populations, differential reddening, rotation effects, etc. This result shows that the age-metallicity diagnostic diagram returns accurate ages at low expense, since it does not require deep photometry nor deal with the known 4-parameter degeneracy (age, metallicity, distance, reddening) when matching isochrones to the cluster CMDs. On the metallicity arena, the derived iron to hydrogen ratios are within $\Delta([\text{Fe/H}]) = \pm 0.15$ dex of the identity relation (see Fig. 7), no systematic dependence with the metallicity taken from the literature is visible along the considered range. Such a dispersion is also comparable to the smallest error atainable in deriving metal abundances from photometric data. The most discrepant point in Fig. 7 corresponds to NGC 6791, which is simply due to a drop in the metallicity sensitivity for metal-rich clusters older than 5 Gyr.

These results reveal that the diagnostic diagram is able to solve the constrains found in the δT_1 index, namely, the loss of age sensitivity for ages greater than $\sim$ 6 Gyr and the strong dependence on both age and metallicity for ages smaller than $\sim$ 5 Gyr. Indeed, as for metal-poor and old clusters, the loss of age sensitivity in δT_1 is surpassed when the δC - δT_1 index is used as a variable instead of the age as proposed by G97 (see top left-hand panel of Fig. 2). Such a choice also allows to obtain a metallicity estimate. For ages younger than $\sim$ 5 Gyr, the diagnostic diagram shows that while δT_1 depends on the age and on the metallicity, δC - δT_1 is mainly a metal abundance indicator, so that the latter fixes the metallicity level where the former is evaluated.

In addition to the δT_1 age calibration, the M_{T_1} versus $(C - T_1)_o$ CMD was also calibrated in terms of metallicity by Geisler & Sarajedini (1999), who demonstrated the metallicity sensitivity of the standard giant branch (SGB, each giant branch corresponds to an iso-abundance curve) applicable to objects with ages $\gtrsim$ 5 Gyr, any age effects are small or negligible for such objects. However, the SGBs were defined for [Fe/H] < -0.5 dex using globular clusters older than 10 Gyr, so that it is important to examine as closely as possible the effect of applying such a calibration to much younger clusters. In view of the well-known age-metallicity degeneracy, Bica et al. (1998) explored this effect empirically by comparing SGB-based metallicities for 11 clusters with ages between 1 and 3 Gyr to standard values. They found a relatively constant offset of $\sim$ 0.4 dex, the SGB metallicities were underestimated due to the effects of age for clusters younger than $\sim$ 3 Gyr. Geisler et al. (2003) investigated this effect in much more detail by using theoretical isochrones computed by Lejeune & Schaerer (2001) for two metallicity

levels ([Fe/H] = -1.3 dex and -0.7 dex). They found that not only a constant offset of ~ 0.4 dex but an exponential correction increasing towards younger ages is necessary. Particularly, they adopted the theoretical prediction for [Fe/H] = -0.7 dex as the correction to be applied to the SGB metallicities as a function of age. Including all error sources, the corrected [Fe/H] values are estimated with an uncertainty of σ([Fe/H]) = 0.3 dex, although the steepness of the age correction for the youngest clusters (< 2 Gyr) results in a larger metallicity error and bias the resulting metallicities upwards.

The referred successive improvements seem surpassed by the new age-metallicity diagnostic diagram. The latter can be used without the knowledge of the cluster distance and reddening, which is mandatory in the SGB technique. Likewise, the diagnostic diagram allows not only to estimate directly more precise metallicities but also ages, simultaneously. The new procedure is subject of no correction and useful for a wide range of ages (1 - 13 Gyr) and metallicities ([Fe/H] = -2.0 - +0.5 dex). All these feature make the diagnostic diagram a powerful tool for estimating accurate ages as well as metallicities.

5 CONCLUSIONS

The Washington photometric system has long been used to estimate ages and metallicities of clusters, particularly for those older than ~ 1 Gyr. Nevertheless, these estimates have relied on calibrations (δT_1 and SGB methods) which involve clusters with ages and metallicities that need to be updated. Likewise, the well-known age-metallicity degeneracy has not been properly addressed or even not considered at all.

We have profusely exploited synthetic T_1 versus $C - T_1$ CMDs with the aim of improving our knowledge about the intrinsic behaviour of the δT_1 index with age and metallicity. The synthetic CMDs were produced through the `ASteCA` suit of functions, taking into account the total cluster mass as a function of age in order to have the MSTO and the RC similarly populated to those known low mass clusters. Photometric errors were also considered, so that the resulting cluster CMDs achieved the appearance of the observed ones.

The analysis of the δT_1 index as a function of the age for different metallicity levels shows that it varies with age and metal content as well. In general, the dependence on age weakens for ages greater than ~ 6 Gyr, and results even less sensitive to age as the metallicity decreases ([Fe/H] $\lesssim$ -1.0 dex). For ages younger than ~ 5 Gyr δT_1 shows a strong correlation with both age and metallicity. As expected, the δC index -defined as δT_1 for C the passband - is also a combined measurement of age and metallicity.

We introduce a new age-metallicity diagnostic diagram, δT_1 versus δC - δT_1, which has shown the ability of unambiguously providing age and metallicity estimates, simultaneously, within certain Washington CT_1 photometric error limits. The proposed technique does not require any additional measurement from other Washington passbands, but only the same CT_1 photometry needed to measure the former δT_1 index. The new procedure allows to derive ages and metallicities within a considerable wide range (age: 1 - 13 Gyr, [Fe/H]: -2.0 - +0.5 dex), and is independent of the cluster reddening and distance modulus. It does solve the constraints found in the δT_1 index and surpasses the performance of the SGB method.

ACKNOWLEDGEMENTS

This work was partially supported by the Argentinian institutions CONICET and Agencia Nacional de Promoción Científica y Tecnológica (ANPCyT). We are grateful for the comments and suggestions raised by the anonymous referee which helped us to improve the manuscript.

REFERENCES

Anthony-Twarog B. J., Twarog B. A., Mayer L., 2007, AJ, 133, 1585
Balaguer-Núñez L., Galadí-Enríquez D., Jordi C., 2007, A&A, 470, 585
Baumgardt H., Parmentier G., Anders P., Grebel E. K., 2013, MNRAS, 430, 676
Beasley M. A., Brodie J. P., Strader J., Forbes D. A., Proctor R. N., Barmby P., Huchra J. P., 2004, AJ, 128, 1623
Bica E., Geisler D., Dottori H., Clariá J. J., Piatti A. E., Santos, Jr. J. F. C., 1998, AJ, 116, 723
Bragaglia A., Carretta E., Gratton R., D'Orazi V., Cassisi S., Lucatello S., 2010, A&A, 519, A60
Bressan A., Marigo P., Girardi L., Salasnich B., Dal Cero C., Rubele S., Nanni A., 2012, MNRAS, 427, 127
Canterna R., 1976, AJ, 81, 228
Carraro G., Chiosi C., 1994, A&A, 287, 761
Casagrande L., VandenBerg D. A., 2014, MNRAS, 444, 392
Catelan M., Leyton P. P., Saito R. K., Borissova J., Popescu B., 2014, in Revista Mexicana de Astronomia y Astrofisica, vol. 27, Vol. 44, Revista Mexicana de Astronomia y Astrofisica Conference Series, pp. 65–65
Chabrier G., 2001, ApJ, 554, 1274
Correnti M., Goudfrooij P., Kalirai J. S., Girardi L., Puzia T. H., Kerber L., 2014, ApJ, 793, 121
Da Costa G. S., Hatzidimitriou D., 1998, AJ, 115, 1934
de Grijs R., Goodwin S. P., Anders P., 2013, MNRAS, 436, 136
Dias B., Kerber L. O., Barbuy B., Santiago B., Ortolani S., Balbinot E., 2014, A&A, 561, A106
Donati P., Cocozza G., Bragaglia A., Pancino E., Cantat-Gaudin T., Carrera R., Tosi M., 2015, MNRAS, 446, 1411
Geisler D., Bica E., Dottori H., Claria J. J., Piatti A. E., Santos, Jr. J. F. C., 1997, AJ, 114, 1920
Geisler D., Piatti A. E., Bica E., Clariá J. J., 2003, MNRAS, 341, 771
Geisler D., Sarajedini A., 1999, AJ, 117, 308
Glatt K. et al., 2009, AJ, 138, 1403
—, 2011, AJ, 142, 36
Heiter U., Soubiran C., Netopil M., Paunzen E., 2014, A&A, 561, A93
Hernandez X., Valls-Gabaud D., Gilmore G., 1999, MNRAS, 304, 705
Jiang D., Han Z., Li L., 2014, ApJ, 789, 88
Kerber L. O., Girardi L., Rubele S., Cioni M.-R., 2009, A&A, 499, 697
Kroupa P., 2002, Science, 295, 82

Kroupa P., Tout C. A., Gilmore G., 1993, Monthly Notices of the Royal Astronomical Society, 262, 545
Lejeune T., Schaerer D., 2001, A&A, 366, 538
Li C., de Grijs R., Deng L., 2013, MNRAS, 436, 1497
Li Z., Mao C., Chen L., Zhang Q., 2012, ApJ, 761, L22
Mackey A. D., Payne M. J., Gilmore G. F., 2006, MNRAS, 369, 921
Milone A. P., Bedin L. R., Piotto G., Anderson J., 2009, A&A, 497, 755
Monteiro H., Dias W. S., Caetano T. C., 2010, A&A, 516, A2
Olszewski E. W., Schommer R. A., Suntzeff N. B., Harris H. C., 1991, AJ, 101, 515
Perren G. I., Vázquez R. A., Piatti A. E., 2015, A&A, in press, arXiv:1412.2366
Phelps R. L., Janes K. A., Montgomery K. A., 1994, AJ, 107, 1079
Piatti A. E., 2011a, MNRAS, 416, L89
—, 2011b, MNRAS, 418, L40
—, 2011c, MNRAS, 418, L69
—, 2014, MNRAS, 437, 1646
Piatti A. E., Bica E., 2012, MNRAS, 425, 3085
Piatti A. E., Bica E., Geisler D., Clariá J. J., 2003, MNRAS, 344, 965
Piatti A. E., Clariá J. J., Ahumada A. V., 2004, MNRAS, 349, 641
Piatti A. E., Clariá J. J., Bica E., Geisler D., Ahumada A. V., Girardi L., 2011, MNRAS, 417, 1559
Piatti A. E., Geisler D., 2013, AJ, 145, 17
Piatti A. E., Geisler D., Mateluna R., 2012, AJ, 144, 100
Piatti A. E., Santos J. F. C., Clariá J. J., Bica E., Sarajedini A., Geisler D., 2001, MNRAS, 325, 792
Piatti A. E., Sarajedini A., Geisler D., Gallart C., Wischnjewsky M., 2007, MNRAS, 381, L84
Popescu B., Hanson M. M., 2014, ApJ, 780, 27
Popescu B., Hanson M. M., Elmegreen B. G., 2012, ApJ, 751, 122
Roediger J. C., Courteau S., Graves G., Schiavon R. P., 2014, ApJS, 210, 10
Romeo G., Fusi Pecci F., Bonifazi A., Tosi M., 1989, MNRAS, 240, 459
Rubele S. et al., 2012, A&A, 537, A106
Sabbi E. et al., 2009, ApJ, 703, 721
Salaris M., Weiss A., Percival S. M., 2004, A&A, 414, 163
Sharma S., Borissova J., Kurtev R., Ivanov V. D., Geisler D., 2010, AJ, 139, 878
Suntzeff N. B., Schommer R. A., Olszewski E. W., Walker A. R., 1992, AJ, 104, 1743
von Hippel T., 2005, ApJ, 622, 565

Table 1. Estimated age (Gyr) and metallicity (dex) errors*

[Fe/H]/ age	1.0	2.0	3.2	4.0	5.0	6.3
-2.0	0.20/0.15	0.20/0.20	0.30/0.20	0.50/0.25	0.70/0.20	0.80/0.25
-1.5	0.20/0.15	0.20/0.15	0.25/0.20	0.50/0.25	**0.60/0.25**	**0.70/0.25**
-1.0	**0.20/0.15**	**0.30/0.15**	**0.40/0.25**	**0.60/0.25**	**0.60/0.25**	**0.60/0.25**
-0.5	**0.20/0.15**	**0.25/0.15**	**0.40/0.25**	**0.50/0.20**	**0.50/0.25**	**0.50/0.25**
0.0	**0.15/0.20**	**0.15/0.20**	**0.20/0.20**	**0.40/0.20**	0.40/0.20	0.50/0.40
+0.5	**0.10/0.20**	0.10/0.20	0.20/0.20	0.30/0.20	0.30/0.20	0.40/0.50
[Fe/H]/ age	7.1	8.0	9.0	10.0	11.2	12.6
-2.0	0.60/0.20	0.60/0.15	0.70/0.15	0.70/0.15	**0.70/0.15**	**0.70/0.15**
-1.5	**1.00/0.20**	**1.00/0.15**	**1.00/0.15**	**1.00/0.15**	**1.00/0.15**	**1.00/0.15**
-1.0	**0.80/0.25**	**1.00/0.25**	**1.00/0.25**	**1.00/0.20**	**1.00/0.15**	**1.00/0.15**
-0.5	**0.50/0.20**	**0.70/0.20**	**0.70/0.20**	**0.60/0.20**	0.60/0.20	0.60/0.20
0.0	0.50/0.40	0.50/0.40	0.50/0.40	0.50/0.40	0.50/0.40	0.50/0.40
+0.5	0.80/0.50	0.80/0.50	0.80/0.50	0.80/0.50	0.80/0.50	0.80/0.50

$*$ Errors in age/metallicity were estimated using $\sigma(\delta C) = \sigma(\delta T_1) = 0.05$ mag and $\sigma(\delta C$ - $\delta T_1) = [(\sigma C)^2 + (\sigma T_1)^2]^{1/2} = 0.07$ mag.

Table 2. Cluster parameters taken from the literature used for comparison purposes.

Cluster	Age (Gyr)	Ref.	[Fe/H] (dex)	Ref.	CT_1 data Ref.	Age (Gyr) (this work)	[Fe/H] (dex) (this work)
47 Tuc	13.1 ± 0.9	1	-0.75± 0.04	11	15	13.0 ± 1.0	-0.80 ± 0.30
AM 3	4.9 ± 1.8	2	-0.8 ± 0.4	2	16	4.5 ± 0.7	-0.75 ± 0.40
ESO 121-SC03	9.0 ± 0.7	3	-0.93 ± 0.20	12	17	9.0 ± 1.0	-0.90 ± 0.30
HW 40	2.50 ± 0.35	2	-0.90 ± 0.15	2	16	3.0 ± 0.7	-1.00 ± 0.40
IC 2146	1.55 ± 0.05	4	-0.4 ± 0.2	4	18	1.5 ± 0.3	-0.60 ± 0.25
Lindsay 3	1.2 ± 0.3	2	-0.40 ± 0.15	2	19	1.3 ± 0.2	-0.50 ± 0.15
Lindsay 113	4.0 ± 0.7	2	-1.24 ± 0.11	2	20	3.5 ± 0.3	-1.20 ± 0.30
NGC 339	6.0 ± 0.5	5	-1.08 ± 0.12	5	16	5.2 ± 1.0	-1.00 ± 0.40
NGC 419	1.4 ± 0.2	6	-0.67 ± 0.12	13	21	1.3 ± 0.3	-0.75 ± 0.30
NGC 2682	4.2 ± 0.2	7	0.00 ± 0.06	23	15	4.2 ± 1.0	-0.10 ± 0.30
NGC 6791	7.0 ± 1.0	8	0.42 ± 0.05	23	15	7.5 ± 0.8	0.00 ± 0.50
SL 509	1.2 ± 0.2	9	-0.54 ± 0.09	9	17	1.0 ± 0.2	-0.40 ± 0.15
SL 862	1.7 ± 0.2	9	-0.47 ± 0.10	9	17	1.7 ± 0.4	-0.50 ± 0.25
Trumpler 5	3.0 ± 1.0	10	-0.40± 0.05	10	22	3.0 ± 0.5	-0.40 ± 0.15

Ref.: (1) Roediger et al. (2014); (2) Dias et al. (2014); (3) Mackey, Payne & Gilmore (2006); (4) Milone et al. (2009); (5) Glatt et al. (2011); (6) Glatt et al. (2009); (7) Balaguer-Núñez, Galadí-Enríquez & Jordi (2007); (8) Anthony-Twarog, Twarog & Mayer (2007); (9) Sharma et al. (2010); (10) Donati et al. (2015); (11) Bragaglia et al. (2010); (12) Olszewski et al. (1991); (13) Da Costa & Hatzidimitriou (1998); (14) Suntzeff et al. (1992); (15) Geisler & Sarajedini (1999); (16) Piatti (2011a); (17) Bica et al. (1998); (18) Piatti (2011b); (19) Piatti et al. (2011); (20) Piatti et al. (2007); (21) Piatti (2011c); (22) Piatti, Clariá & Ahumada (2004); (23) Heiter et al. (2014).

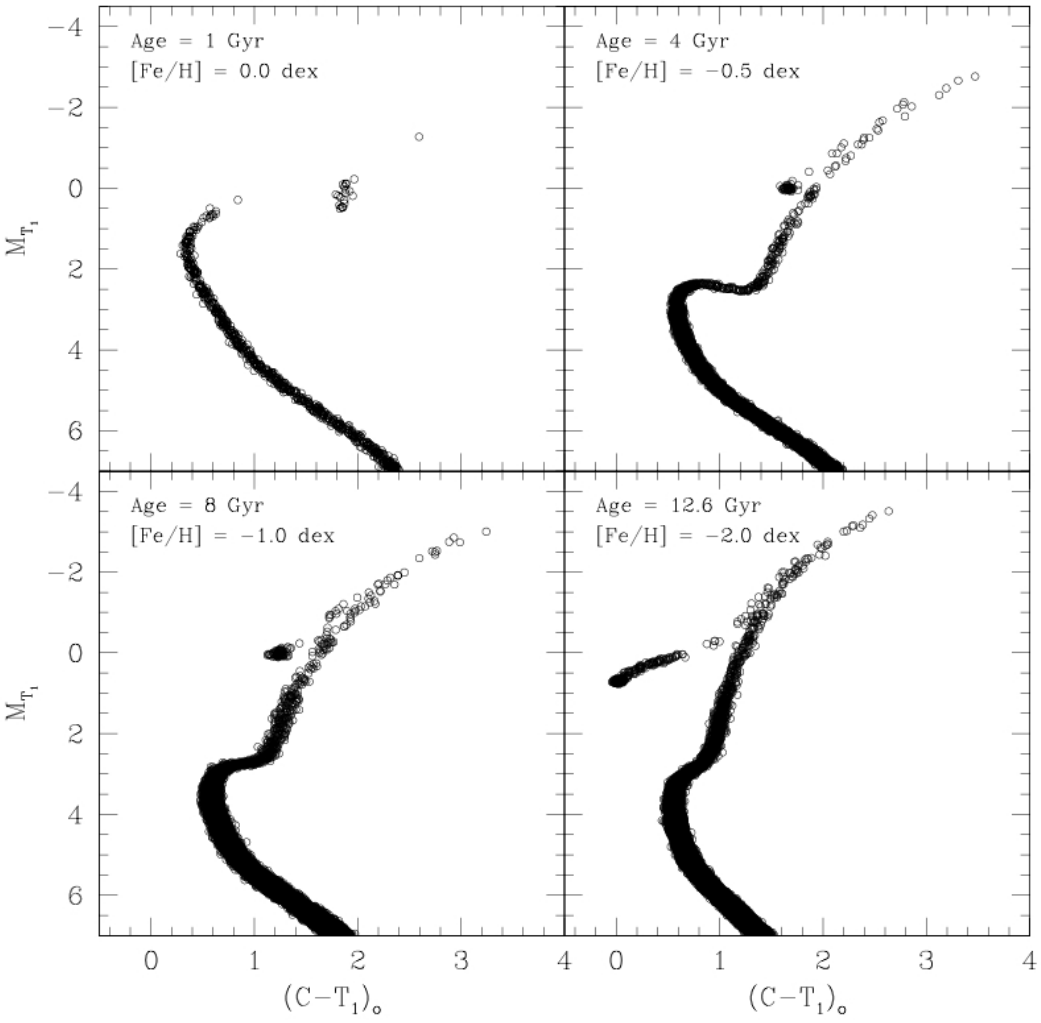

Figure 1. Examples of synthetic CMDs produced using the `ASteCA` suit of functions.

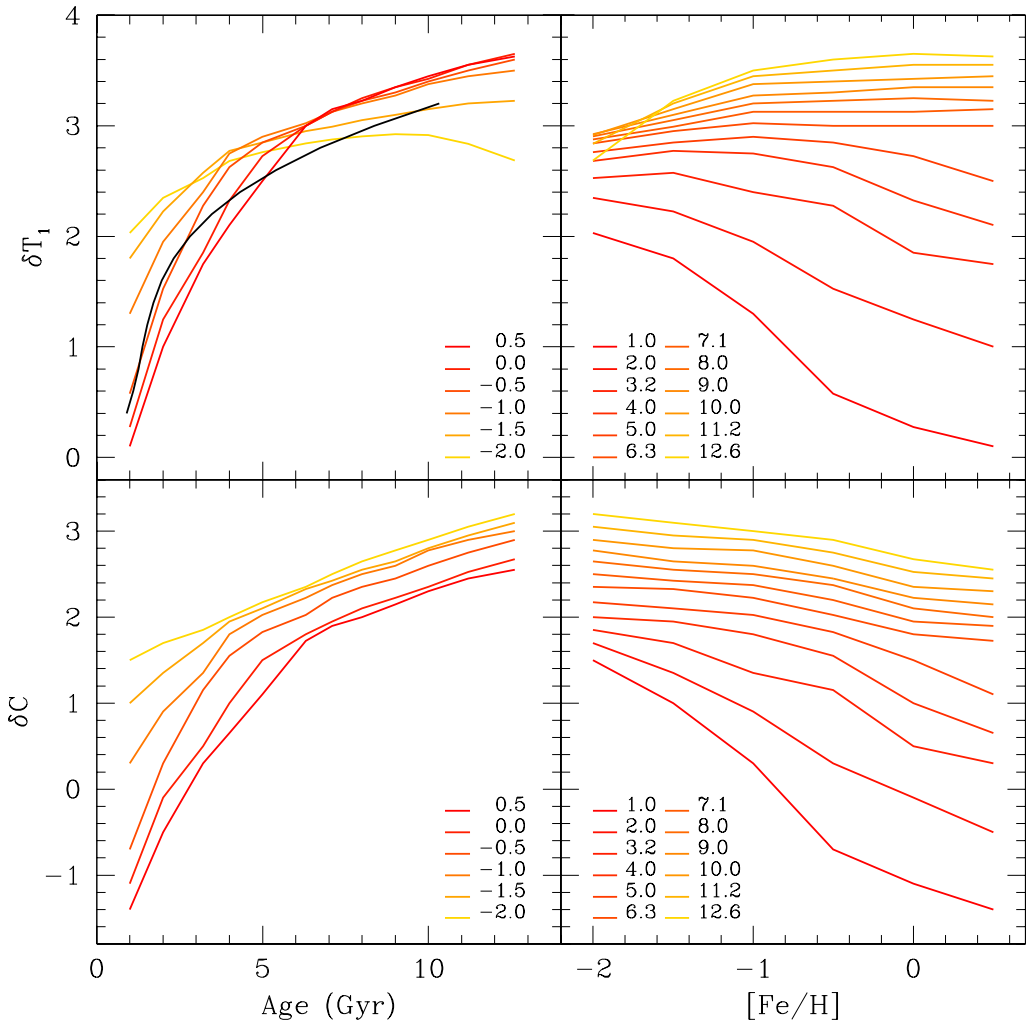

Figure 2. Relationship of δC and δT_1 indices with the age for different [Fe/H] (dex) values (left-hand panels) and with the metallicity for different ages (Gyr) (right-hand panels). The black curve in the upper left-hand panel corresponds to the G97's calibration.

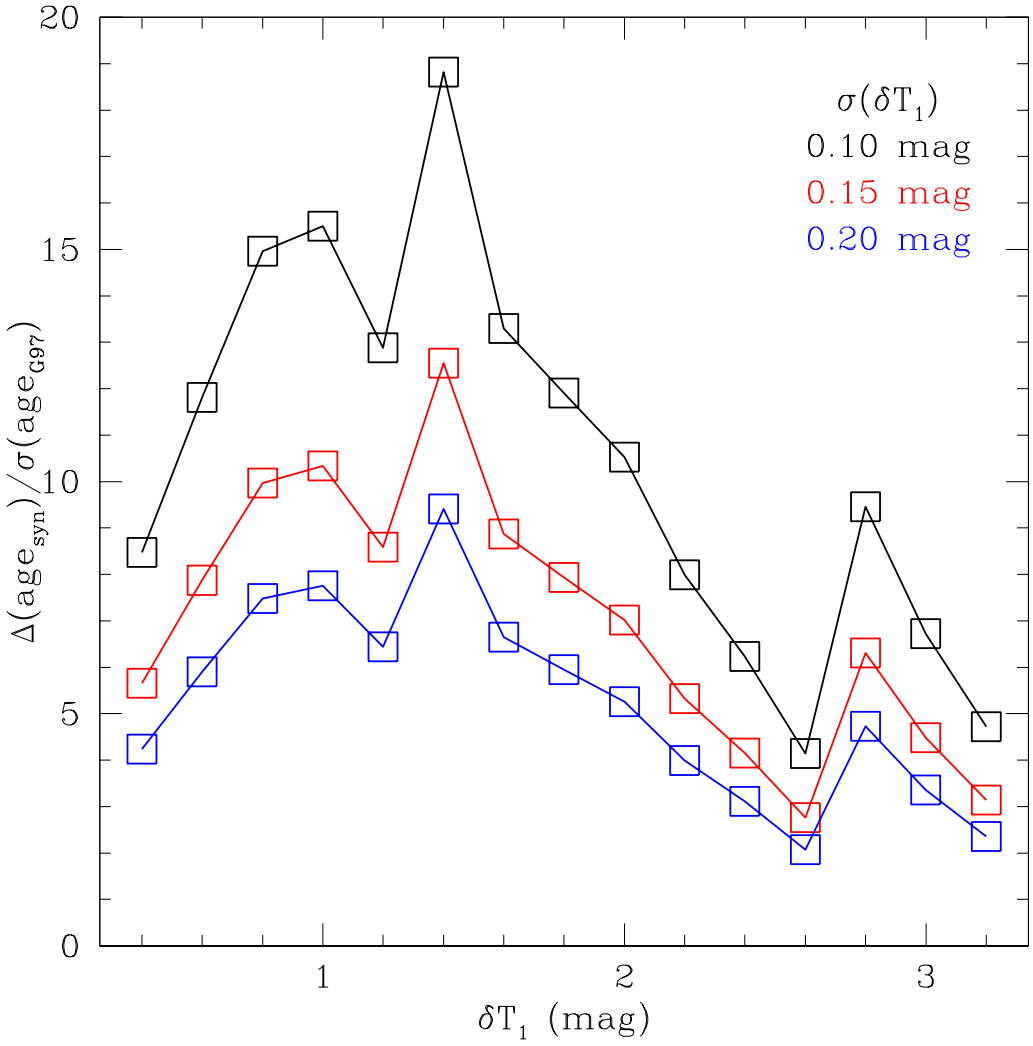

Figure 3. Synthetic age range to $\sigma(\mathrm{age}_{G97})$ ratio as a function of δT_1.

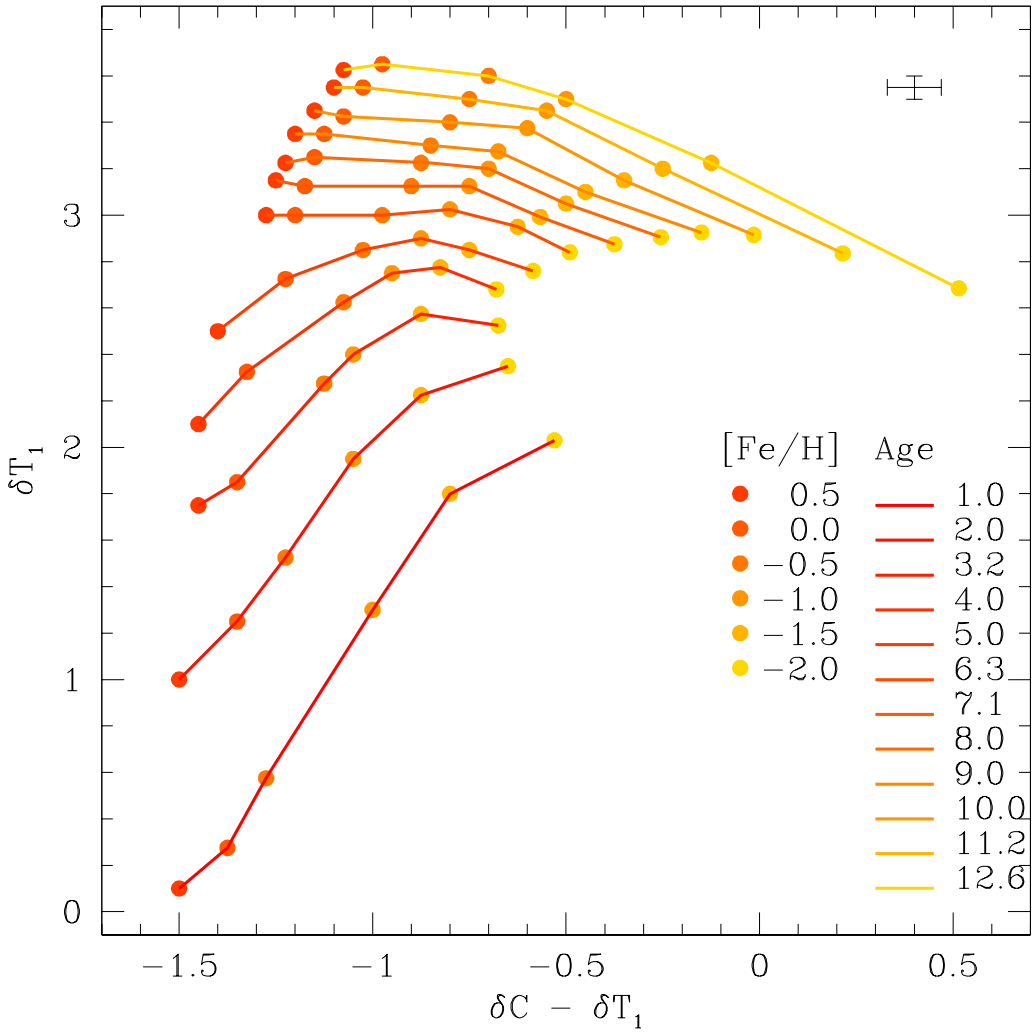

Figure 4. δT_1 versus δC - δT_1 diagram with iso-age lines and iso-metallicity locii. Metallicity and age labels are given in dex and Gyr, respectively.

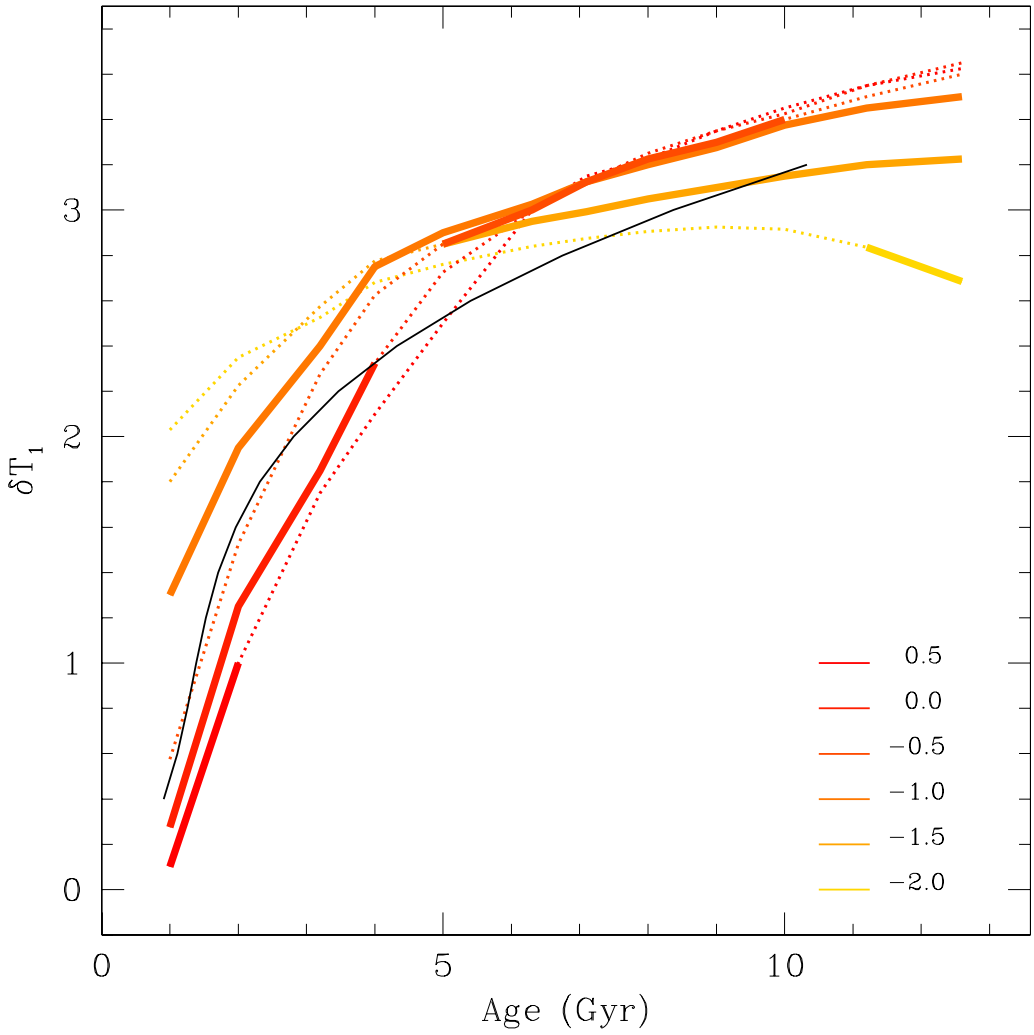

Figure 5. Same as Fig. 2 (upper left-hand panel), where thick line sections correpond to ages/metallicities with uncertainties in boldface characters in Table 1.

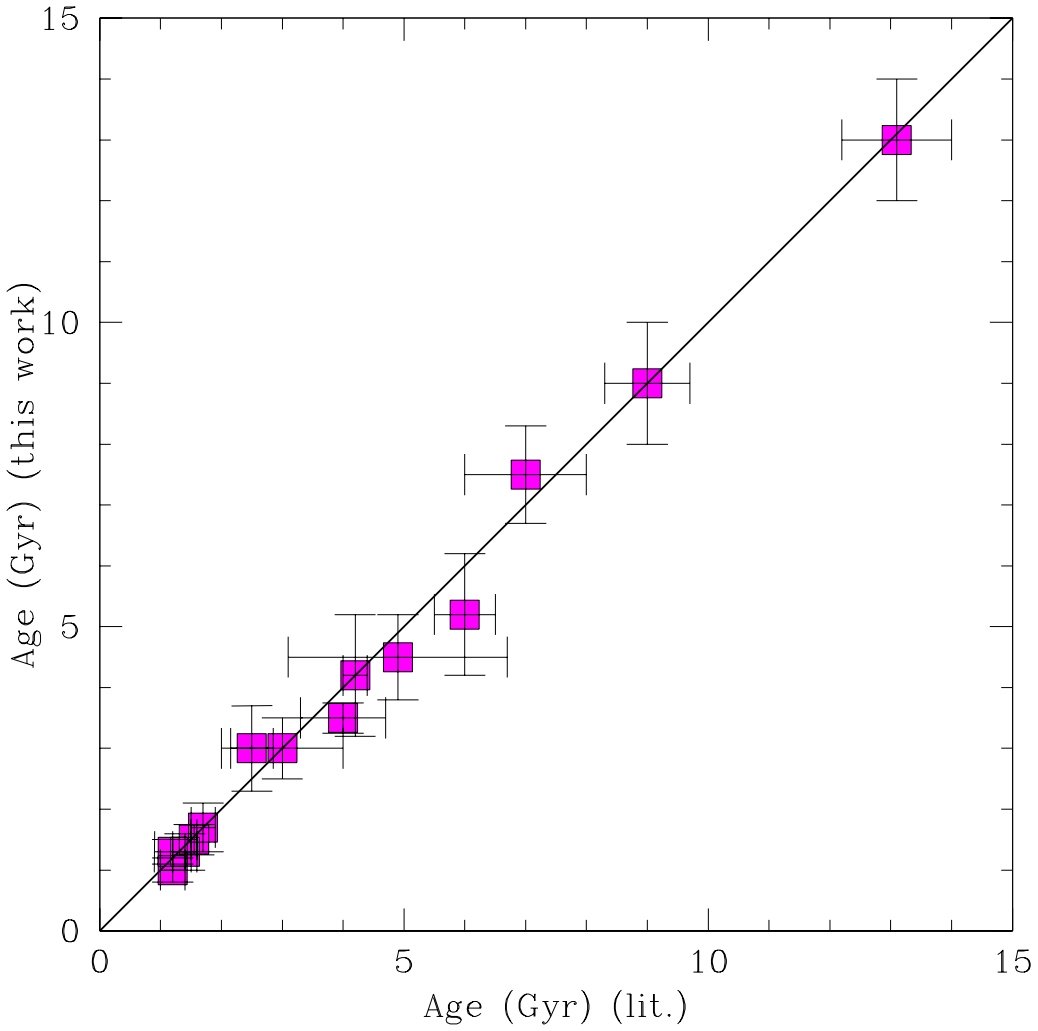

Figure 6. Comparison between ages taken from the literature and estimated using the age-metallicity diagnostic diagram.

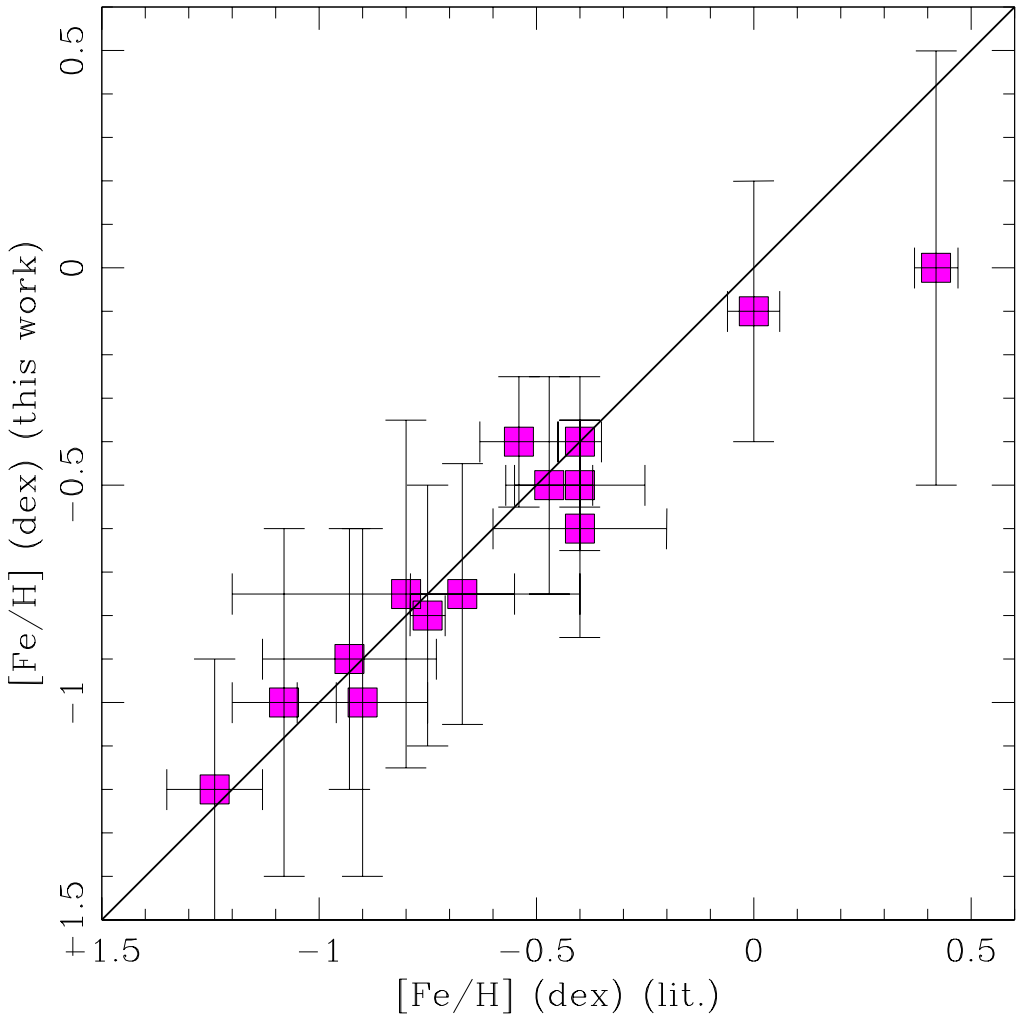

Figure 7. Comparison between metallicities taken from the literature and estimated using the age-metallicity diagnostic diagram.